Ocean Science Journal, Vol. 43 No. 2, 115-126(2008)

Note

Ocean Science Journal

http://osj.kr

Direct Observation of Radiative Flux in the Southern Yellow Sea

Lü Lian-Gang*, Yu Fei, Diao Xinyuan, Guo Jingsong, Wang Huiwu, and Wei Chuanjie

Laboratory of Marine Science and Numerical Modeling, the First Institute of Oceanography, State Oceanic Administration, Qingdao 266061, China

Received 2 January 2008; Revised 12 May 2008; Accepted 15 June 2008

Abstract – Direct measurements of four radiative components at air-sea boundary layer were conducted in the southern Yellow Sea during three cruises (seasons) in 2007. Simultaneous observations of meteorological (cloud cover, air temperature and humidity) and oceanographic (sea surface temperature) parameters were carried out. Observational results of radiative fluxes and meteorological and oceanographic parameters are presented. Mean diurnal cycles of four radiative components, net radiation, and sea surface albedo are calculated to achieve averages in different seasons. Net radiative fluxes in three seasons (winter, spring, autumn) are 8, 146, 60 W/m^2, respectively. Comparisons between the observed radiative fluxes and those estimated with formulas are taken.

Key words – radiative flux, net radiation, air-sea boundary layer, Yellow Sea

1. Introduction

Heat flux at air-sea boundary layer has a large effect on the global weather system, oceanic and atmospheric circulations. The total heat flux consists of both radiative fluxes and turbulent fluxes. Radiation is usually divided into shortwave and longwave components. As shortwave, the solar radiation is the major energy source for the earth and atmosphere. The solar radiant energy absorbed by the atmosphere and the earth surface heats the earth-atmosphere climate system and drives atmosphere movement. All components of climate system emit longwave radiant energy according to the Stefan-Boltzmann law (Peixoto and Oort 1992). At air-sea boundary layer, radiative fluxes consist of four components: downward and upward shortwave radiation, and downward and upward longwave radiation.

Direct radiative observations have been carried out in the eastern Pacific Ocean (Reed and Halpern 1975; Reed 1977), the North Pacific Ocean (Simpson and Paulson 1979), the North Tyrrhenian Sea (Schiano *et al*. 1993), the western Mediterranean Sea (Bignami *et al*. 1995), the Northeast Atlantic and the Southern Ocean in the vicinity of the Azores (Josey *et al*. 1997), the South China Sea (Jiang *et al*. 2002), and the east Atlantic (Josey *et al*. 2003). Some of these studies have reported simultaneous measurements of four radiative components (Simpson and Paulson 1979; Schiano *et al*. 1993; Jiang *et al*. 2002). An overestimate of the downward longwave caused by heating of the dome with solar radiation has been identified (Fairall *et al*. 1998; Pascal and Josey 2000); this has contributed to accurate measurement of radiative flux in recent years. Direct measurements of radiative fluxes are usually with incomplete spatial and temporal coverage. Therefore, many studies have been made in order to derive empirical formulas, which form the basis for estimating the radiative flux at the air-sea boundary layer (*e.g*. Lumb 1964; Payne 1972; Clark *et al*. 1974; Reed 1977; Shine 1984; Dobson and Smith 1988; Bignami *et al*. 1995; Josey *et al*. 2003). One can refer to a summary about radiative flux parameterization by Kantha and Clayson (2000). Being important to modeling the evolution of the atmosphere and ocean, accurate parameterization of radiative fluxes needs direct observation of radiation.

Direct observation of radiative flux in the Yellow Sea is infrequent. Hirose *et al*. (1999) reported the shortwave and estimated longwave radiation fluxes estimated with

*Corresponding author. E-mail: lvlg@fio.org.cn

Comprehensive Ocean Atmosphere Dataset (COADS) in the Yellow Sea and East China Sea. Chu *et al*. (2005) studied seasonal variability of the Yellow Sea and East China Sea surface fluxes and investigated the linkage between the surface fluxes and the formation of the water mass features. The radiative fluxes were directly obtained from the COADS dataset. Byun and Cho (2006) explored the daily and seasonal variability in the ratio of photosynthetically active radiation to total irradiance that occurred at Ieodo Ocean Research Station the in the East China Sea under clear-sky conditions.

The multidisciplinary oceanographic investigation was carried out in the southern Yellow Sea. As a part of this investigation, flux measurements at air-sea boundary layer have been made. This paper gives the results of radiative flux observation in the southern Yellow Sea during three cruises in 2007. The goal of this study is to report radiative fluxes at air-sea boundary layer in different seasons and give comparisons between the measured and estimated radiation with formulas. Research cruises, instrumentation and data acquisition are described in section 2. Results of the observation during three cruises are presented in section 3. Section 4 gives mean of radiative fluxes in different seasons. Section 5 consists of comparisons between measured and estimated radiation with formulas. The final section is a summary.

2. Observations

Research cruises

The multidisciplinary oceanographic investigation was conducted in the southern Yellow Sea during three cruises (seasons) in 2007. In these cruises, radiation measurements were carried out continuously when the ship was either under way, at a hydrographic station, or anchored for shelter. Stations of radiative observation are shown in Figure 1. Cruises 1 and 3 were carried out on R.V. Beidou from Jan. 8 to Feb. 5 (winter), and from Oct. 6 to Nov. 5 (autumn), respectively. Cruise 2 was made on R.V. Kexue1 from Apr. 3 to 27 (spring). Observations were firstly carried out in Qingdao coastal area during all cruises. Then, cruises 1 and 3 were made from the south to the north, and cruise 2 was in the opposite direction. From Jan. 23 to 27, and 29 to 30, R.V. Bedou made harbor due to strong winds. It rained on Jan. 12, 15, and 16 during cruise 1. Continuous heavy fog occurred on Apr. 7 and 8 during cruise 2. It rained in the afternoon of Apr. 15. During cruise 3, R.V. Bedou made harbor from Oct. 7 to 10, 11 to 14, and 27 to 29. Rain occurred on Oct. 7, 11, and 25.

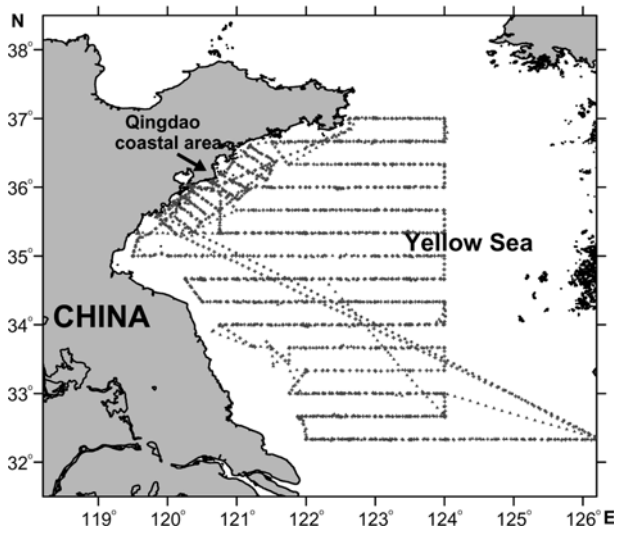

Fig. 1. Stations of radiative observation during cruise 1, 2, and 3.

Instrumentation and data acquisition

Observation system of air-sea fluxes included a three dimensional sonic anemometer, an open path CO_2/H_2O analyzer, a temperature and relative humidity probe (HMP45C), an infrared thermocouple sensor (IRR-P), two pyranometers, two pyrgeometers, and two measurement and control units. One unit collected radiative data from four radiometers while the other collected raw data from sonic anemometer, CO_2/H_2O analyzer, HMP45C and IRR-P. All data were recorded on the disks of computers, which were connected to the measurement and control units.

Two pyranometers are used to measure the downward shortwave radiation (DSR) from the solar and atmosphere diffusion, and the upward shortwave radiation (USR) reflected by sea surface. The radiant energy is converted into a voltage by a thermal detector in the pyranometer. The detector of the pyranometer is shielded by two glass domes. Limited by the transmission of the glass, the spectral range of the pyranometer is 310-2800 nm. Two pyrgeometers are used to measure the downward longwave radiation (DLR) from the atmosphere and the upward longwave radiation (ULR) form the sea surface. The pyrgeometer is provided with a silicon window to shield the detector and pass long wave radiation only. The spectral range of the pyrgeometer is 4.5-40 μm. The pyrgeometer temperature variations

between window and sensor are less than 0.3 degrees Celsius, which represent a window heating offset less than 4 W/m^2.

The temperature and relative humidity probe (HMP45C) uses Platinum resistance temperature detector to measure temperature and a capacitive relative humidity sensor to measure relative humidity. The air temperature and humidity measured with the HMP45C can be used to estimate longwave from atmosphere. The infrared temperature sensor (IRR-P) is a non-contact means of measuring the surface temperature of an object by sensing the infrared radiation being emitted by the target. The IRR-P includes a thermopile for measuring a millivolt output dependent on the target to sensor body temperature difference. Wavelength range of the IRR-P is 8 to 14 μm. An air purge is used to keep the lens and view clean. The sea surface temperature measured with IRR-P can be used to calculate longwave from sea surface.

The sensors of the observation system were fastened onto a mast, which was fixed at the end of a horizontal boom. The boom mounted to the ship at a height of about 5 m (R.V. Beidou) or 8 m (R.V. Kexue1) above the water surface is about 5 m length to avoid the disturbance of the ship to the measurements. Four radiometers (2 upper and 2 lower) were mounted to a plate with a 500 mm rod. The rod was fixed at the end of the mast to ensure that a shadow would not be cast on it at any time. The radiometers were leveled by turning the leveling screws to bring the bubble of the spirit level within the marked ring. The HMP45C was housed inside a radiation shield to avoid the influence of solar radiation. The radiation shield mounts to the mast.

Before observation of each cruise, the clocks of computers connected with the measurement and control units were set to synchronize with the Global Positioning System (GPS) time. The clocks of measurement and control units were then synchronized with the computer clocks. Observations of radiation were made at a frequency of 1 Hz and recorded as 10- and 30-minute means. The air temperature, relative humidity, vapor pressure (estimated with air temperature and relative humidity), and sea surface temperature were measured at a frequency of 10 Hz and recorded as 10- and 30-minute means. Meteorological observations were carried out with shipboard aerograph. Meteorological data with 3-second interval, and their 1-minute, hour, day means were recorded. Note that cloud cover was visually estimated only during the day with a 1- or 2-hour interval (at hydrographic stations, and at local hour 8 and 14 when the ship was cruising).

Radiometers were checked and cleaned regularly, especially when the investigation ship was departing from harbor, and after rain or heavy fog. The system power was switched off during heavy rain or strong winds. Any events of radiative importance were recorded in radiation log.

3. Results

Radiative data measured in harbor are rejected according to time, latitude and longitude data from GPS. Radiative data recorded during rain, heavy fog, or cleaning time are removed according to meteorological observations and radiative observation log. To control the quality of data, air temperature and humidity are compared to that measured by shipboard aerograph, and infrared sea surface temperature is compared to sea temperature at 1 m depth measured by CTD. Data of 30- minute mean are used in this paper.

Cruise 1

Results of four radiative components and meteorological and oceanographic parameters including cloud cover, infrared sea surface temperature, air temperature, and vapor pressure observed during cruise 1 are presented in Fig. 2. Since R.V. Bedou made harbor due to strong winds, no observations were conducted from Jan. 23 to 27, and data recorded from Jan. 29 to 30 (in harbor) are removed. Radiative data measured from Jan. 15 to 16 were rejected due to continuous rain. From 0830 to 1510 on Feb. 3, the boom was taken back because of large waves. The recorded data during that time were removed.

The DSR showed a pronounced daily variation with high values (on the order of 100-700 W/m^2) in daytime and zero in nighttime. The USR ranged from 0 (in nighttime) to 70 W/m^2 (in daytime) with a conspicuous diurnal variation. Lower values of shortwave were observed on Jan. 12, 14, 22, 28, and 31.

The DLR ranged from 260-360 W/m^2, and the ULR ranged from 340-400 W/m^2. The DLR and ULR had the same order of magnitude. But the ULR was always higher than the DLR. The longwave budget led to sea heat loss. Low frequency variation of the ULR decreased with time.

Infrared sea surface temperature ranged from 2 to 16 °C. Its variability was close to that of the ULR. Given emissivity for the surface, the ULR is a function of surface temperature given by the Stefan-Boltzmann law. Thus, sea surface

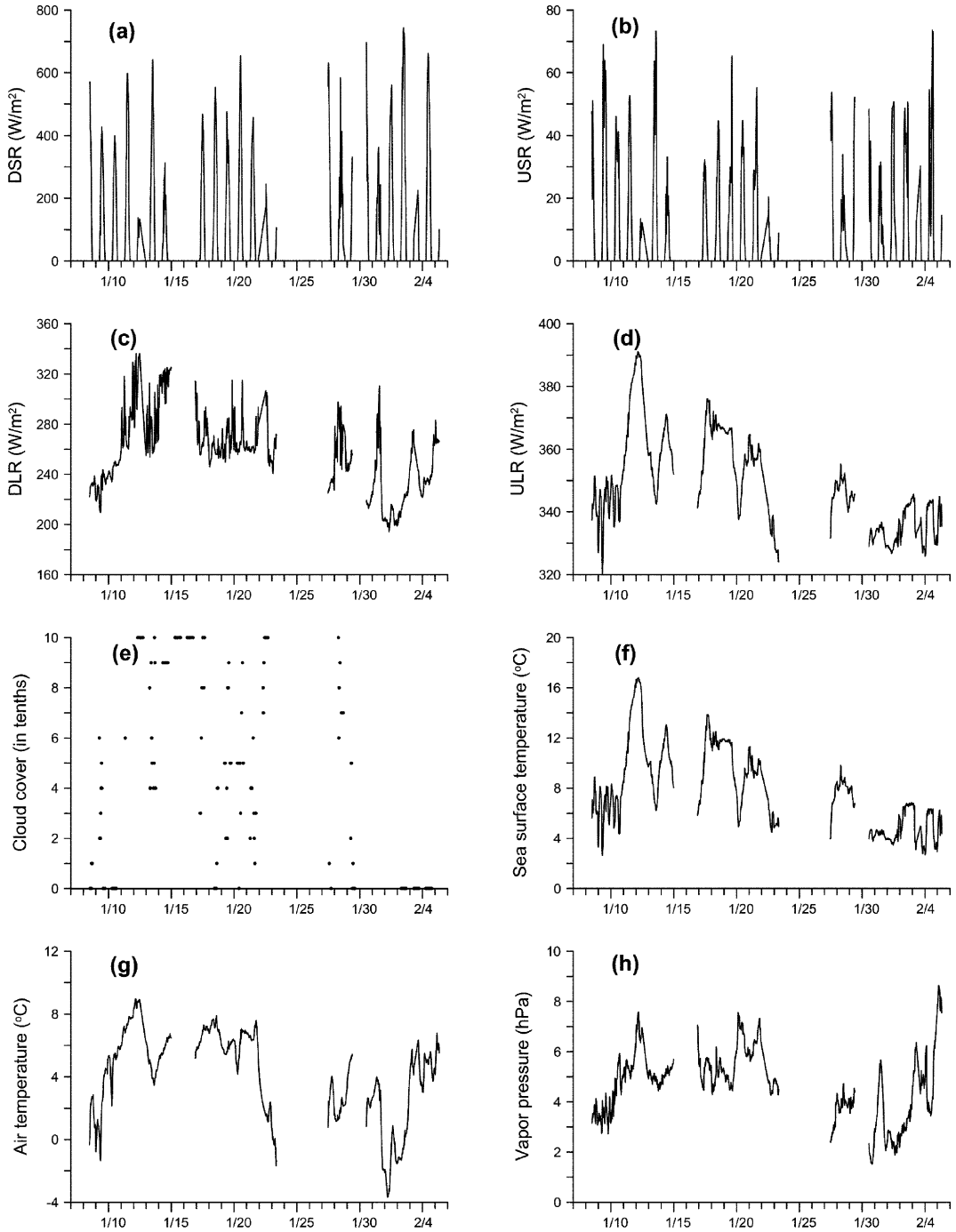

Fig. 2. Time series of the various radiative components and meteorological and oceanographic parameters observed during cruise 1 in 2007: (a) downward shortwave radiation (DSR), (b) upward shortwave radiation (USR), (c) downward longwave radiation (DLR), (d) upward longwave radiation (ULR), (e) cloud cover, (f) infrared sea surface temperature, (g) air temperature, and (h) vapor pressure. Time is expressed in month/day.

temperature and the ULR measured during cruise 1 presented similar variations. Cruise 1 was made from the southern part of focused area where sea surface was higher to the northern part where sea surface was lower. As a result, the ULR decreased gradually with time.

High cloud cover occurred on Jan. 12, 14, 22, and 28, while the low DSR and peaks of the DLR existed. This showed the influence of cloud cover on the DSR and the

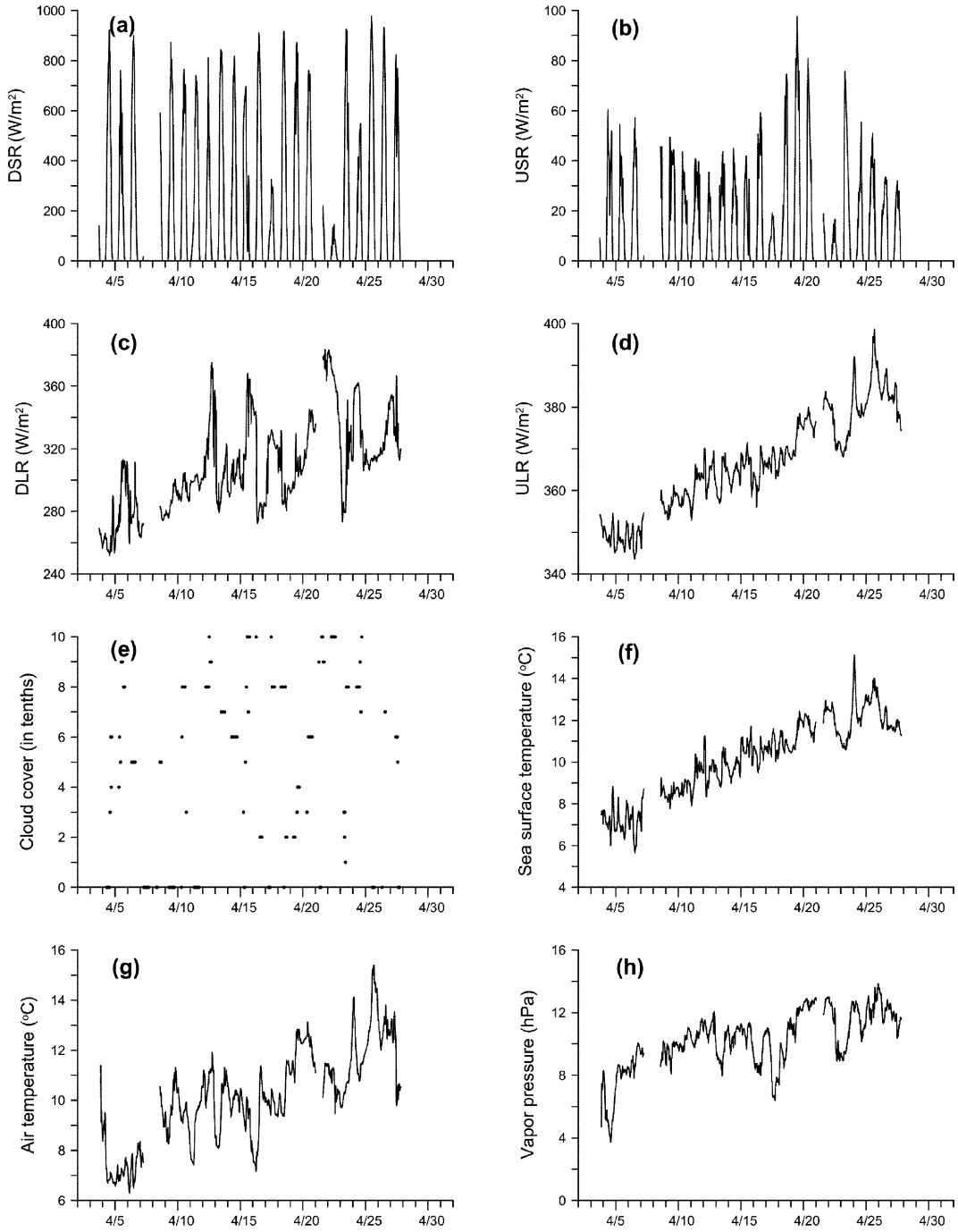

Fig. 3. As figure 2, but observed during cruise 2 in 2007.

DLR. Scattering inside the clouds dominates the depletion of solar radiation. The DLR depends on the vertical temperature profile, the clouds, and the vertical distribution of the absorbers. In some parameterization methods, the DLR is a function of cloud, the temperature and humidity of the air near the surface. High cloud cover results in high longwave radiation, and the warmer or more humid the air, the higher the longwave radiation at the surface.

Air temperature lay in range from -4 to 9 °C. It decreased quickly on Jan. 31 while the DLR decreased also. This revealed the effect of air temperature on the DLR. The influence of vapor pressure (ranging from 2-9 hPa) was obvious in that its peaks occurred on Jan. 12, 31, Feb. 3, and 5 when the peaks of the DLR existed.

Cruise 2

Radiative, meteorological and oceanographic results observed during cruise 2 are presented in Fig. 3. Data recorded from Apr. 7 to 8, and on Apr. 21 were removed due to heavy fog. As expected, shortwave radiation was characterized by a prominent daily variation. The DSR measured during this cruise was higher than that observed during cruise 1. The DSR values in daytime reached 900 W/m^2, and the highest USR was over 90 W/m^2. Lower values of shortwave were observed on Apr. 17, 22, and 24.

The DLR (260-380 W/m^2) and the ULR (340-400 W/m^2) were higher than those measured during cruise 1, respectively. As that in cruise 1, the ULR was always higher than the DLR. The DLR and ULR increased gradually with time due

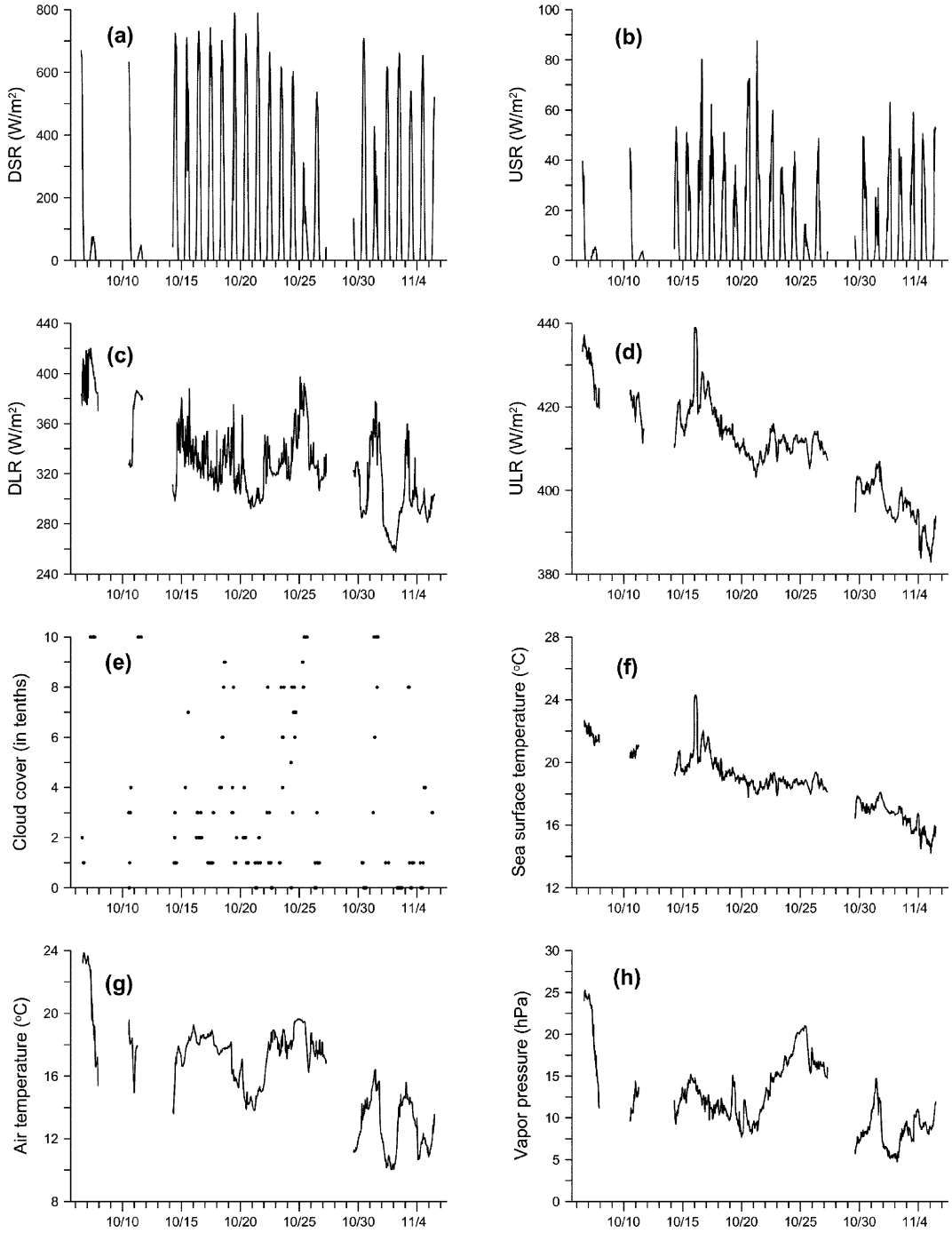

Fig. 4. As figure 2, but observed during cruise 3 in 2007.

to the north-to-south cruise.

High cloud cover occurred on Apr. 5, 12, 15, 17, 22 and 24. This resulted in peaks of the DLR. The influence of cloud on the DSR was obvious on Apr. 17, 22, and 24.

Vapor pressure, air and sea surface temperature increased gradually with time because of the north-to-south cruise as mentioned in Section 2. These led to increase of the DLR and ULR. Vapor pressure and air temperature were higher than that measured during cruise 1.

Cruise 3

The DSR reached 700 W/m^2 in several days, and the USR ranged from 0-80 W/m^2 (Fig. 4). Shortwave radiation measured during this cruise was lower than that observed during cruise 2, and somewhat higher than that in cruise 1. Lower values of shortwave were observed on Oct. 7, 11, 25, and 31 when peaks of the DLR and high cloudiness occurred. No observations were conducted from Oct. 8 to 10, 11 to 14, and 27 to 29 because R.V. Beidou stayed in harbor due to strong winds.

The DLR (260-420 W/m^2) and the ULR (380-440 W/m^2) were higher than those measured during the previous cruises due to higher vapor pressure, air and sea surface temperature. Similar to that measured in the previous two cruises, the ULR was always higher than the DLR. Due to the south-to-north cruise direction, vapor pressure, air and sea surface temperature, and the consequent DLR and ULR decreased gradually with time.

4. Mean Radiative Fluxes in Different Seasons

The radiative flux observed in three cruises (seasons) show differences. To quantify the differences of radiation in three seasons, means of four radiative components, net radiation, and sea surface albedo should be calculated. Net radiation (RN) is the difference between the downward and upward radiation (RN=DSR+DLR–USR–ULR). The surface albedo is defined as the ratio of the USR over the DSR. In nighttime the albedo is zero due to no solar radiation. The DSR, USR, RN, and albedo have obvious daily variations. Amounts of data in daytime and nighttime are not equal. Therefore, their means cannot be calculated by summarizing the data directly. In this case, authors calculate mean diurnal cycles (a single day data from averaging synchronous data in different days) of the DSR, USR, DLR, ULR, RN, and albedo (Fig. 5 and 6) firstly. The means of the DSR, USR, DLR, ULR, RN, and albedo in different seasons are computed with 48 data that denote the mean diurnal cycles in Fig. 5 and 6 (30-minute means used in this study) and are listed in Table 1.

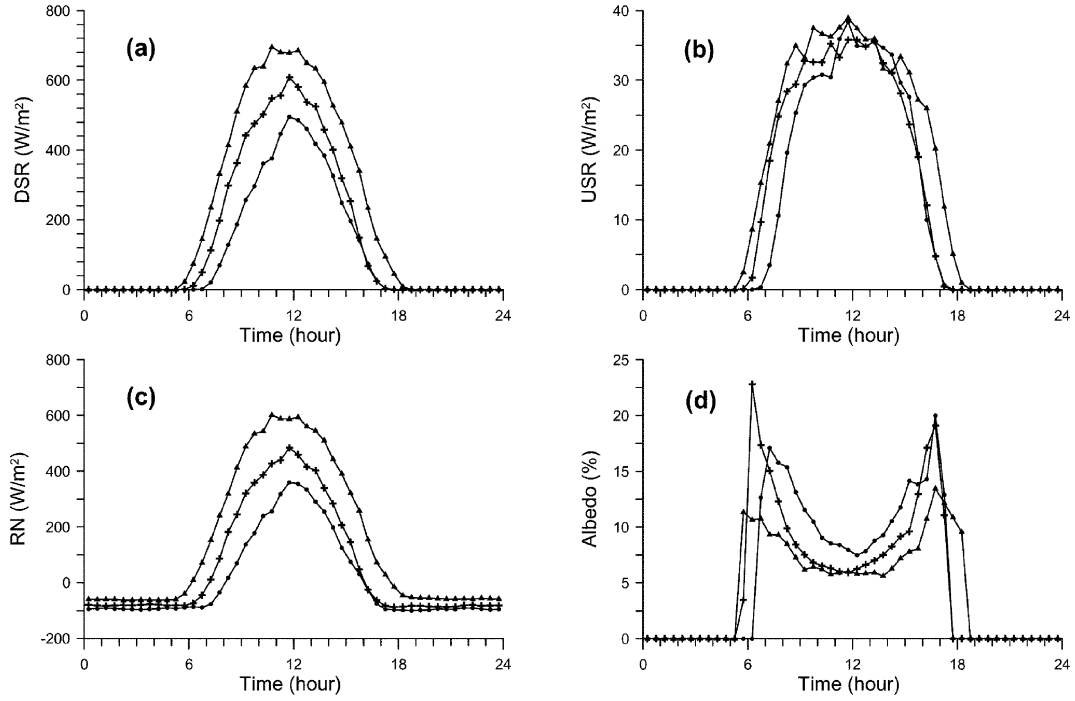

Fig. 5. Mean diurnal cycles of the (a) DSR, (b) USR, (c) RN, and (d) reflectivity of shortwave (Albedo) in cruise 1 (dot line), 2 (triangle line), and 3 (cross line).

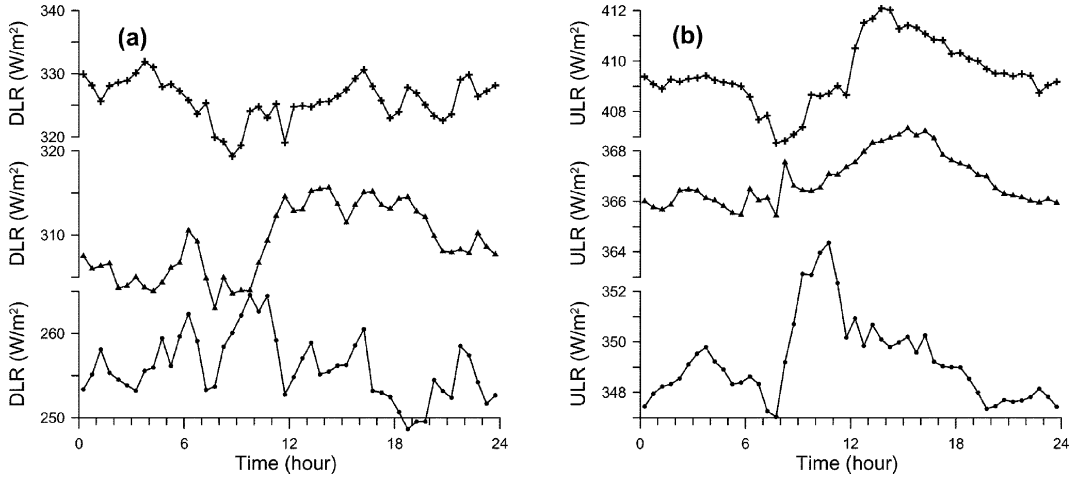

Fig. 6. Mean diurnal cycles of the (a) DLR, and (b) ULR in cruise 1 (dot line), 2 (triangle line), and 3 (cross line).

Table 1. Means of radiative fluxes during three cruises

Cruise	DSR (W/m^2)	USR (W/m^2)	DLR (W/m^2)	ULR (W/m^2)	RN (W/m^2)	Albedo (%)
1	112.5	10.8	256.0	349.2	8.4	5.4
2	218.5	14.4	309.1	366.8	146.4	4.4
3	155.9	11.9	325.8	409.5	60.3	5.1

The DSR, USR, RN, and sea surface albedo are symmetric about noon (Fig. 5), as expected. Differences of the DSR in three seasons are obvious. The DSR in autumn is lower than that in spring, and higher than that in winter. The USR do not show seasonal difference as obvious as the DSR because the USR depends on not only the DSR but also the surface reflectivity (albedo). The albedo, which is depends on the sea state and the solar zenith angle (Payne 1972; Kantha and Clayson 2000; Jiang *et al*. 2002), shows seasonal variation contrary to that of the DSR (Fig. 5d). The highest albedo occurs in winter when the DSR is the lowest. The albedo always has a minimum near noon in daytime. The RN, which is dominated by the DSR, shows seasonal difference similar to the DSR (Fig. 5c). The longwave in spring is higher than that in winter, and lower than that in autumn (Fig. 6). Daily variation of the DLR (about 15 W/m^2) is greater than that of the ULR (about 5 W/m^2). In spring and autumn, the longwave increases slightly near noon.

Table 1 gives the means of radiative fluxes during three cruises (seasons). The seasonal variations of the USR, DSR and RN are uniform (low in winter, high in spring, medium in autumn). The lowest solar radiation occurs in winter while seawater loses most heat due to longwave (about 93 W/m^2). The RN in winter is lowest in three seasons. In spring, daily solar radiation is over 200 W/m^2, and the longwave denotes the least sea heat loss (about 58 W/m^2). These give rise to highest RN in three seasons. In autumn, heat loss resulting from the longwave budget is about 84 W/m^2.

5. Parameterization

Downward shortwave radiation

Lumb (1964) formula is suitable to estimate hourly DSR,

$$DSR = S_0 \cos\theta_z (\mathrm{A} + B\cos\theta_z) \tag{1}$$

where S_0 is the solar constant, θ_z is the solar zenith angle, and A, B are coefficients dependent on nine categories of cloud types. The zenith angle is given by (Zhang and Anthes, 1982).

$$\cos\theta_z = \sin\ \psi \sin\delta + \cos\psi \cos\delta \cos h \tag{2}$$

where ψ is the latitude (north positive), δ is the declination, and h is the hour angle:

$$\delta = 0.409\cos\left[\frac{2\pi(J_d - 173)}{365.25}\right]$$
$$h = \pi\left(\frac{T_{UTC}}{12} + \frac{lon}{180} - 1\right) \tag{3}$$

J_d is the day of the year, T_{UTC} is the Coordinated Universal Time in hours, and *lon* is the longitude in degree (east positive).

Based on more data, Dobson and Smith (1988) have suggested different coefficients for Lumb formula. The coefficients depend on cloud types. Simply, only the DSR under the clear sky is computed using Lumb formula with the coefficients given by Dobson and Smith (1988). Byun and Pinardi (2007) have shown that earth–sun distance effect should be considered in solar irradiance formulas. We use Spencer's (1971) algorithm for the earth–sun distance correction factor γ^2 in this work,

$$\gamma^2 = 1.00011 + 3.4221\times10^{-2}\cos(A_d) + 1.28\times10^{-3}\sin(A_d) + 7.19\times10^{-4}\cos(2A_d) + 7.7\times10^{-5}\sin(2A_d) \quad (4)$$

The day angle is equal to

$$A_d = \frac{2\pi}{365}(J_d - 1) \quad (5)$$

The result that contains a total of 233 comparisons from three cruises is shown in Fig. 7. The root mean square error is 87.4 W/m^2, and the mean bias error is 5.0 W/m^2. The formula overestimates at fluxes greater than 800 W/m^2. The DSR depends on the solar zenith angle, aerosol, water vapor, and cloud cover (Kantha and Clayson 2000). The present estimation only deals with the solar zenith angle and cloud (clear sky). The difference between estimation and observation results from the influence of the aerosol and water vapor in some degree.

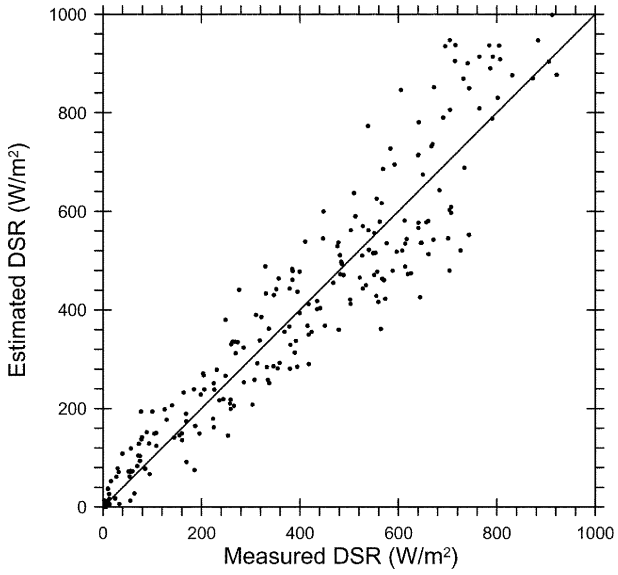

Fig. 7. Scatterplot of estimated versus measured DSR under clear sky from three cruises.

Albedo

Payne (1972) has suggested a table of the sea surface albedo as a function of solar altitude (θ) and atmospheric transmittance (T) defined as

$$T = DSR/(S_0 \sin\theta/\gamma^2) \quad (6)$$

The DSR is the measured downward shortwave radiation. The sum of altitude angle and zenith angle equals 90°. Thus, the solar altitude θ is computed with the solar zenith angle (calculated with equation 2 and 3). The earth–sun distance correction factor γ^2 is calculated with equation 4 and 5.

Surface albedo values are computed from Payne (1972) table with solar altitude and atmospheric transmittance. If the computed solar altitude or atmospheric transmittance is beyond the table limits, the albedo is zero. Mean diurnal cycles of albedo are computed (Fig. 8) as described in section 4. The estimated albedo in winter is lower than the observed except values in later afternoon. In spring and autumn, the estimated albedo values are also lower except that in early morning and later afternoon. The difference between estimation and observation is apparent at dawn and dusk while the USR is at low value and relative error is at high value. This perhaps results in the obvious difference at dawn and dusk. The estimated albedo values are symmetric about noon. The averages of the estimated albedo from mean daily cycles (Fig. 8) are 4.8%, 4.3%, and 4.5% in three seasons (winter, spring, autumn), lower than the observed albedo in Table 1. This is possibly due to difference in measurement platform (fixed platform used in Payne study and ship used in our observation). Seasonal variation of estimated albedo is similar to that of the observed (compared to Table 1).

Downward longwave radiation

Several formulas have been proposed to compute the longwave radiation from the atmosphere. Josey *et al*. (1997) have compared the DLR observed in the North Atlantic and the Southern Ocean to estimations with Clark *et al*. (1974), Bunker (1976), and Bignanmi *et al*. (1995) formulas. In that comparison, cloud cover data are extracted from the Comprehensive Ocean Atmosphere Dataset 1a

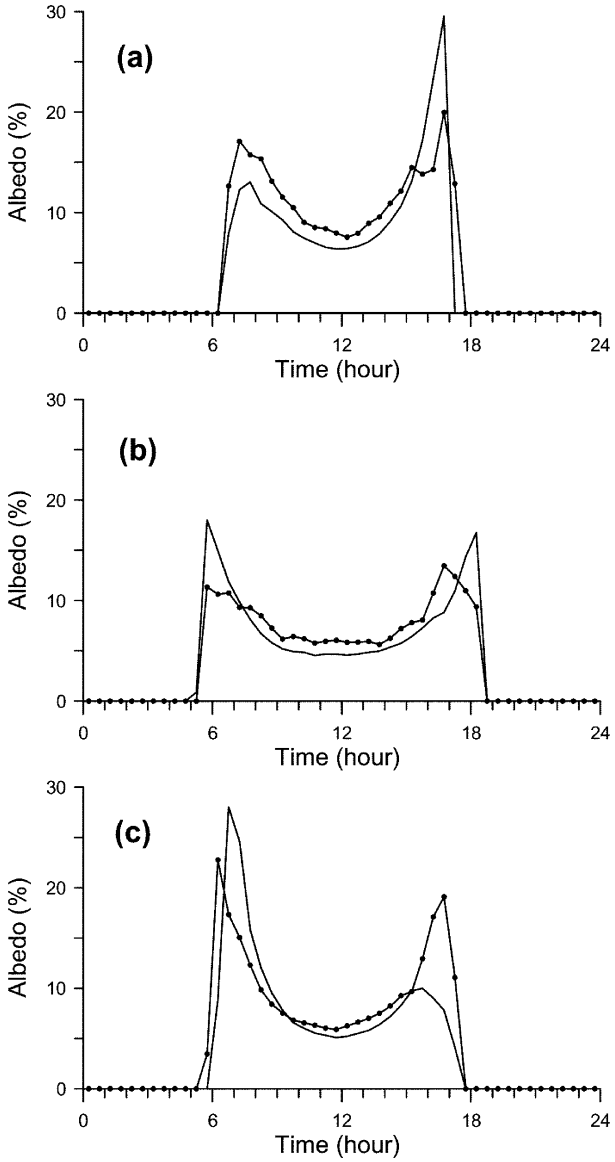

Fig. 8. Mean diurnal cycles of the estimated albedo (line), and the observed (dot line, replotted from Fig. 5) in cruise 1 (a), 2 (b), and 3 (c).

(COADS 1a). The Clark formulation is recommended to be used at midlatitudes due to its least bias (The root mean square error of 886 comparisons is 15.8 W/m^2). Therefore, we use Clark formula to estimate the DLR with cloud cover, vapor pressure, sea surface and air temperature observed. Since cloud cover was visually observed only during the day time, linear interpolation is used to produce 30-miniute-interval cloud cover data. Latitude-dependent cloud cover coefficient (Josey *et al.* 1997) is taken to be 0.67.

The result that contains a total of 2724 comparisons from three cruises is shown in Fig. 9. The Clark formula performs

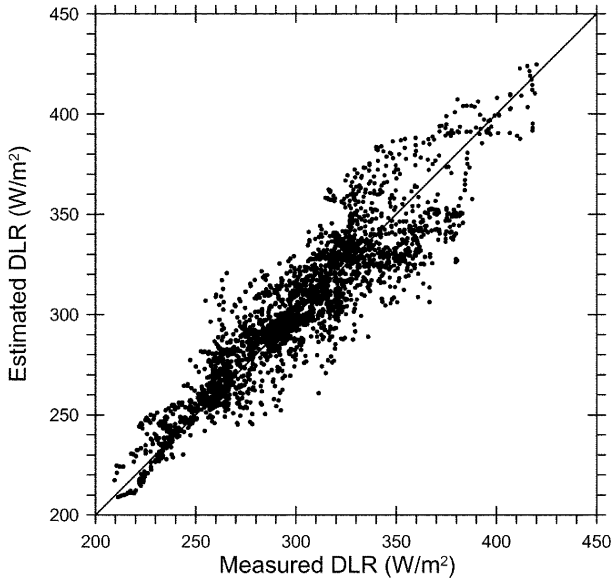

Fig. 9. Scatterplot of estimated versus measured DLR from three cruises.

well with the mean bias error of 1.1 W/m^2 and the root mean square error of 15.8 W/m^2. The root mean square error of 1330 (1394) comparisons based on daytime (nighttime) data is 14.9 (16.7) W/m^2. This denotes the importance of cloud observation. The visual observation of cloud leads to the error to some extent.

Upward longwave radiation

The upward longwave radiation consists of the component emitted by the sea surface and the component of DLR

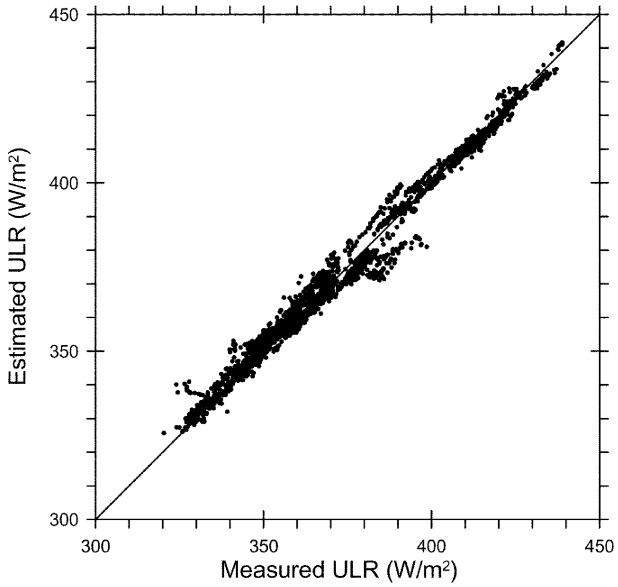

Fig. 10. Scatterplot of estimated versus measured ULR from three cruises.

reflected from the sea surface (Kantha and Clayson 2000),

$$ULR = \varepsilon\sigma T_s^4 + \alpha_l DLR \quad (7)$$

Where ε is the surface emissivity, σ is the Stefan-Boltzmann constant, T_s is the surface temperature, and α_l is the longwave reflectivity. Here, ε is taken to be 0.98, and α_l is taken to be 0.02. Figure 10 shows comparison between the estimated and measured ULR. The root mean square error is 3.5 W/m^2. As described in section 2, the surface temperature is measured with a non-contact means by sensing the infrared radiation being emitted by the sea surface. The measured result with the non-contact means is easily influenced by weather. The difference in the ULR between estimation and observation is possibly due to the non-contact means of temperature measurement.

6. Summary

Direct observations of radiative flux and meteorological and oceanographic parameters at air-sea boundary have been carried out in the southern Yellow Sea during three cruises in 2007. Cruises were made from Jan. 8 to Feb. 5 (winter), from Apr. 3 to 27 (spring), and from Oct. 6 to Nov. 5 (autumn), respectively. Primary results are reported to give an overview of seasonal variations of radiation and the influence of meteorological and oceanographic parameters on the radiative flux in the southern Yellow Sea. Mean diurnal cycles are calculated to achieve averages of radiative variables in different seasons. In spring, solar radiation is higher than that in winter and autumn, and sea heat loss resulting from the longwave budget is low. These lead to high net radiative flux in this season. Seasonal variation of albedo is contrary to that of the DSR. Net radiative fluxes in three seasons (winter, spring, autumn) are 8, 146, 60 W/m^2, respectively.

Comparisons between the measured and estimated radiative components are taken. The DSR values under the clear sky are calculated using Lumb (1964) formula with the coefficients given by Dobson and Smith (1988). The root mean square error is 87.4 W/m^2. The averages of estimated albedo from Payne (1972) model are 4.8%, 4.3%, and 4.5% in three reasons (winter, spring, autumn), lower than those measured. The DLR estimated with Clark formula is compared to that observed during three cruises. The root mean square error of 2724 comparisons is 15.8 W/m^2. Comparison between the estimated and measured ULR results in a mean square error of 3.5 W/m^2.

Acknowledgements

This work is supported by program (908-ZC-I-01) and program (2007G13).

References

Bignami, F., S. Marullo, R. Santoleri, and M.E. Schiano. 1995. Longwave radiation budget in the Mediterranean Sea. *J. Geophys. Res*., **100**, 2501-2514.

Bunker, A.F. 1976. Computations of surface energy flux and annual air-sea interaction cycles of the North Atlantic Ocean. *Mon. Wea. Rev*., **104**(9), 1122-1140.

Byun, D.-S. and Y.-K. Cho. 2006. Estimation of the PAR irradiance ratio and its variability under clear-sky conditions at Ieodo in the East China Sea. *Ocean Sci. J.*, **41**(4), 235-244.

Byun, D.-S. and N. Pinardi. 2007. Comparison of marine insolation estimating methods in the Adriatic Sea. *Ocean Sci. J.*, **42**(4), 211-222.

Clark, N.E., L. Eber, R.M. Laurs, J.A. Renner, and J.F.T. Saur. 1974. Heat exchange between ocean and atmosphere in the eastern North Pacific for 1961-71. NOAA Tech. Rep. NMFS SSRF-682, U.S. Dep. Commer., Washington, D.C.

Chu, P., Y. Chen, and A. Kuninaka. 2005. Seasonal variability of the Yellow Sea/East China Sea surface fluxes and thermohaline structure. *Adv. Atmos. Sci.*, **22**(1), 1-20.

Dobson, F.W. and S.D. Smith. 1988. Bulk models of solar radiation at sea. *Quart. J. R. Met. Soc*., **114**, 165-182.

Fairall, C.W., P.O.G. Persson, E.F. Bradley, R.E. Payne, and S.P. Anderson. 1998. A new look at calibration and use of Eppley precision infrared radiometers Part I: theory and application. *J. Atmos. Ocean. Tech*., **15**, 1230-1243.

Hirose, N., H.-C. Lee, and J.-H. Yoon. 1999. Surface heat flux in the East China Sea and the Yellow Sea. *J. Phys. Oceanogr.*, **29**(3), 401-417.

Jiang, G., W. Sha, J. Yan, X. Li, Y. Xiao, H. Yao, J. Li, and Z. Lu. 2002. The analysis of the radiation features before and after South China Sea monsoon onset. *J. Tropi. Mete*., **18**, 29-37.

Josey, S.A., D. Oakley, and R.W. Pascal. 1997. On estimating the atmospheric longwave flux at the ocean surface from ship meteorological reports. *J. Geophys. Res*., **102**, 27961-27972.

Josey, S. A., R.W. Pascal, P.K. Taylor, and M.J. Yelland. 2003. A new formula for determining the atmospheric longwave flux at the ocean surface at mid-high latitudes. *J. Geophys. Res*., **108**, DOI 10.1029/2002JC001418.

Kantha, L.H. and C.A. Clayson. 2000. Small-scale processes in geophysical fluid flows. Academic Press, New York. 888 p.

Lumb, F.E. 1964. The influence of cloud on hourly amounts of total solar radiation at the sea surface. *Quart. J. R. Met. Soc*., **90**, 43-56.

Pascal, R.W. and S.A. Josey. 2000. Accurate radiometric measurement of the atmospheric longwave flux at the sea surface, *J. Atmos. Ocean. Tech*., **17**, 1271-1282.

Payne, R.E. 1972. Albedo of the sea surface. *J. Atmos. Sci*., **29**, 959-970.

Peixoto, J.P. and A.H. Oort. 1992. Physics of climate. Springer-Verlag, New York. 520 p.

Reed, R.K. 1977. On estimating insolation over the ocean. *J. Phys. Oceanogr*., **7**, 482-485.

Reed, R.K. and D. Halpern. 1975. Insolation and net longwave radiation off the Oregon Coast. *J. Geophys. Res*., **80**, 839-844.

Schiano, M.E., R. Santoleri, F. Bignami, R.M. Leonardi, S. Marullo, and E. Bohm. 1993. Air-sea interaction measurements in the west Mediterranean Sea during the Thyrrhenian Eddy Multi-Platform observations experiment. *J. Geophys. Res.*, **98**, 2461-2474.

Shine, K.P. 1984. Parameterization of the shortwave flux over high albedo surfaces as a function of cloud thickness and surface albedo. *Quart. J. R. Met. Soc*., **110**, 747-764.

Simpson, J.J. and C.A. Paulson. 1979. Mid-ocean observations of atmospheric radiation. *Quart. J. R. Met. Soc*., **105**, 487-502.

Spencer, J.W. 1971. Fourier series representation of the position of the Sun. *Search*, **2**(5), 172.

Zhang, D. and R.A. Anthes. 1982. A high-resolution model of the planetary boundary layer-sensitivity tests and comparisons with SESAME-79 data. *J. Appl. Meteor*., **21**, 1594-1609.